Innovative Turbine Stator Well Design Using Design Optimisation

Julien Pohl, Harvey Thompson, Ralf Schlaps, Shahrokh Shahpar, Vincenzo Fico, Gary Clayton

Innovative Turbine Stator Well Design Using Design Optimisation

Julien Pohl[1]*, Harvey Thompson[1], Ralf Schlaps[2], Shahrokh Shahpar[3], Vincenzo Fico[3], Gary Clayton[3]

ISROMAC 2016

International Symposium on Transport Phenomena and Dynamics of Rotating Machinery

Hawaii, Honolulu

April 10-15, 2016

Abstract

Nowadays, it is common practice to expose engine components to main annulus air temperatures exceeding the thermal material limit in order to increase the overall engine performance and to minimise the engine specific fuel consumption. To prevent overheating of the materials and thus the reduction of component life, an internal flow system is required to cool and protect the critical engine parts. Previous studies have shown that the insertion of a deflector plate in turbine cavities leads to a more effective use of reduced cooling air, since the coolant is fed more effectively into the disc boundary layer.

This paper describes a flexible design parameterisation of an engine representative turbine stator well geometry with stationary deflector plate and its implementation within an automated design optimisation process using automatic meshing and steady-state CFD. Special attention and effort is turned to the flexibility of the parameterisation method in order to reduce the number of design variables to a minimum on the one hand but increasing the design space flexibility & generality on the other. Finally the optimised design is evaluated using a coupled FEA/CFD method and compared against the baseline design.

Keywords

Turbine Stator Well — Internal Cooling — CFD — Automated meshing — Kriging — Optimisation

[1] *School of Mechanical Engineering, University of Leeds, Leeds, United Kingdom*

[2] *School of Engineering and Material Science, Queen Mary University of London, London, United Kingdom*

[3] *Rolls-Royce plc., Derby, United Kingdom*

***Corresponding author**: j.pohl@leeds.ac.uk

NOMENCLATURE

Abbreviations

AMEDEO	Aerospace Multidisciplinary Enabling Design Optimisation
ARMOGA	Adaptive Range Multi-Objective Genetic Algorithm
CAD	Computer Aided Design
CFD	Computational Fluid Dynamics
CGEI	Constraint Generalised Expected Improvement
DOE	Design of Experiments
FEA	Finite Element Analysis
HPC	High Performance Computing
LHS	Latin Hypercube Sampling
MAGPI	Main Annulus Gas Path Interaction
RANS	Reynolds-Averaged Navier-Stokes
RSM	Response Surface Model
SQP	Sequential Quadratic Programming
TSW	Turbine Stator Well

Symbols

d, l	[-]	Geometrical design variables
f	[-]	Objective function
g	[-]	Constraint
$\dot{m}_{cool}$	$[\mathrm{kg\,s^{-1}}]$	Cooling mass flow rate
n	[-]	Number of design variables
r	[m]	Radius
Re_ϕ	[-]	Rotational Reynolds number
t	[m]	Thickness
T_{disc}	[K]	Adiabatic disc temperature
T_{fl}	[K]	Relative fluid temperature
T_m	[K]	Metal temperature
v_θ	$[\mathrm{m\,s^{-1}}]$	Tangential velocity
$\mathbf{x}$	[-]	Design vector
y^+	[-]	Non-dimensional near wall spacing
β	[-]	Swirl ratio
ω	$[\mathrm{rad\,s^{-1}}]$	Rotational speed

INTRODUCTION

Over the last decades the significance of internal cooling air systems have become increasingly important in the field of modern gas turbine engines. The main target for aero-engine manufacturers is an improvement of the overall engine efficiency, and thus a reduction in specific fuel consumption. This is mainly achieved by an increase of temperature of the exhaust gas coming from the combustion chamber, which enters the turbine main gas path. These gas temperatures exceed the thermal material limit of the engine components, both within (i.e. blades) and adjacent (i.e. cavities) to the main gas path. To prevent damage and to protect these components from overheating, secondary cooling air systems are designed. The required cooling air is bled from compressor stages and introduced to the blade cooling channels and the exposed turbine cavities, which are inevitably formed by stationary and rotating walls. In order to maximise the overall cycle performance the minimum cooling air mass flow rate should be used that still ensures the required component life. There are mainly two reasons in favour of a reduction of the cooling air: first, the higher the amount of cooling air, the worse the engine thermodynamic cycle performance. Second, the higher the amount of cooling air re-entering the main gas path at a later stage, the lower is the stage efficiency [1, 2].

As a follow up study of the work carried out during the MAGPI (*Main Annulus Gas Path Interaction*) project, sub-project 7 of the EU FP7 project AMEDEO (*Aerospace Multi-*

disciplinary Enabling Design Optimisation) specifically aims towards the development of a robust design optimisation strategy for turbine stator wells (TSW) in order to improve the cooling performance and reduce the required amount of coolant.

During the last couple of years some of the experimental data obtained during the MAGPI project has been analysed and validated. Dixon *et al.* [3] did some preliminary analyses of different cooling configurations using adiabatic steady-state computational fluid dynamics (CFD) solutions in order to obtain an understanding of the different flow fields inside the cavities. With regard to the cooling effectiveness of the rotor disc and the front cavity, it has been concluded that it is desirable to get an entrainment of the cooling air along the rotor wall. This can be achieved either by axial lock plate inlets or a deflected radial coolant inflow. Similar conclusions have been made by da Soghe *et al.* [4] and Coren *et al.* [5], who conducted parameter studies analysing different positions and inclinations of the radial drive arm hole.

Recently, Pohl *et al.* [6] analysed in detail the test case with a mounted stationary deflector plate in the upstream cavity and proposed different modelling and meshing strategies. Using steady-state CFD, the flow physics as well as the cooling effectiveness on the upstream rotor disc were compared between the baseline (i.e. cavity without deflector) and the deflector plate geometry for two different amounts of coolant mass flow. Since the deflector directs the cooling air towards the disc, even small volumes of cooling air result in an improved cooling performance. It was concluded that the cooling air could nearly be halved by inserting the deflector into the cavity.

In a practical aero engine context, Young *et al.* [7] analysed the effect of a deflector plate attached to the rotating drive arm in order to improve the cooling effectiveness on the rotor disc. It was also found that due to the deflector the cooling air is entrained towards the disc, resulting in better cooling of that particular critical part. The outcome was so promising that it has been patented successfully.

Regarding the development and application of optimisation techniques to aero-engine components a lot of effort has been made in the field of main gas path aerodynamics (e.g. [8–10]). Whereas in main gas path aerodynamics the parameterisation of the blades or vanes is mainly realised by parameterising the main defining engineering parameters, such as chord length, camberline angle, pitch and thickness, the parameterisation of components forming the internal cooling systems is less consolidated.

Verstraete *et al.* [11] parameterised a 2D U-bend geometry, which is typical for internal cooling channels, using third order Bézier curves defined by four control points each. Every control point was given a particular degree of freedom in order to keep the design variables to a minimum but at the same time covering a large design space.

For the automatic optimisation of the baseline MAGPI TSW geometry, Lück *et al.* [12] used a mixture of CAD-based parameterisation and mesh morphing from the output of the evaluation of a thermal-fluid structure interaction. With this approach it was possible to change the inclination of the cooling hole and also take thermo-mechanical effects into account.

In the following sections, first a short overview and introduction is given on the flow physics present in a TSW with a stationary deflector plate. Then, some theoretical background on general optimisation strategies and on response surface modelling approaches are presented. This is followed by the numerical methodology used in this work, consisting of the introduction to the test case geometry and the CFD evaluation technique. The latter includes a description of the discretised CFD model with its basic assumptions for boundary conditions and restrictions, as it is embedded in the automatic meshing process. The parameterisation of the deflector plate geometry with its necessary geometrical approximations is also presented, with the focus on the actual optimisation setup defining the objective function and the constraints. Results obtained from the optimisation are shown, interpreted and discussed. Finally, the main conclusions are drawn and recommendations for future work are given.

THEORETICAL BACKGROUND

TSW Flow Theory

This section gives an overview of the flow behaviour in a TSW with an integrated stationary deflector plate and its benefits compared to a standard baseline geometry without a deflector. A schematic illustration of the typical TSW flow phenomena with an inserted stationary deflector plate can be seen in Fig. 1. The orange and black contour lines represent rotating and stationary parts, respectively. Cooling air is introduced into the upstream cavity radially through a drive arm hole. Other than for the standard geometry, the cooling air does not penetrate the cavity forming a core flow, but instead impinges the deflector plate and is turned towards the rotor disc, by forming a complex 3D vortex flow structure. The cooling air which reaches the disc is then entrained radially outwards by the rotating part of the turbine. The rim seal flow characterises the mixing zone between the hot gas coming from

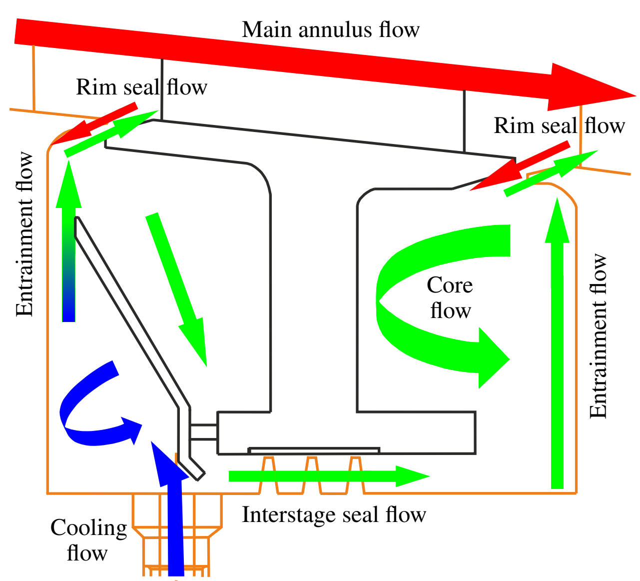

Figure 1. Stator well flow structure with stationary deflector plate

the main annulus and the cooling air. The interaction of these two flows strongly affects the temperatures inside the cavity. Three different flow scenarios can be distinguished depending on the amount of cooling air and the size of the interstage seal clearance [13, 14]:

Net gas ingestion: If the amount of cooling air is small and/or the interstage seal clearance is large, the rim seal flow is dominated by hot gas entering the cavity.

Net gas egress: If the amount of cooling air is large and/or the interstage seal clearance is tight, the rim seal flow is dominated by cooling air leaving the cavity in the main annulus.

Local ingestion/egress: If the cavity flow is balanced locally hot gas enters the cavity but also cool air enters the main annulus. This phenomenon is driven by the rotor-stator interaction in the main gas path and the turbulent mixing in the rim region.

The portion of air/gas mixture staying in the cavity then finds its way to the interstage seal clearance since the deflector plate is mounted to the stator foot by a few pins, spacers or bolts in order to allow air to pass between these parts. This flow is driven by the presence of a pressure gradient from outer to inner radii between the stator wall and the deflector plate. Interstage seals are used to reduce the flow of air from upstream to downstream stator well cavities. This seal flow is, as mentioned above, largely influenced by the clearance size and also the pressure drop across the seal, which is a function of the upstream and downstream conditions including the pressure drop over the stage in the main annulus. The flow structure in the downstream cavity can then again be described as a traditional rotor-stator flow, consisting of a disc entrainment flow, a core flow and a rim seal exchange flow.

Optimisation Theory

Within this subsection, some theoretical background on a typical optimisation strategy is described as it is used for many complex engineering or aero-engine problems. Also, the response surface modelling technique, a method on how to choose the initial database, as well as the actual optimisation method used in this work are presented.

Optimisation Strategy

The optimisation is conducted using the Rolls-Royce SOPHY system (SOFT, PADRAM, HYDRA) [15]. SOFT (Smart Optimisation For Turbomachinery) [16] provides a library of different optimisation algorithms and communicates through python scripts with the other codes in order to execute them in batch mode, to evaluate the results of the simulation. In general, these computations are run in parallel on an HPC cluster in order to reduce the overall run time.

The 2D geometry is generated parametrically using a python programme and then fed to the meshing tool PADRAM (Parametric Design and Rapid Meshing) [17]. PADRAM then generates automatically and robustly 3D structured and unstructured meshes for the main annulus and for the cavity domain, respectively. The discretised 3D model is passed to the HYDRA system [18] for pre-processing and finally solving the Reynolds-Averaged Navier-Stokes equations (RANS). The converged CFD solution is then fed to the post-processing tool Paraview, where the solution is evaluated with respect to the figure of merit, i.e. the objective function, then passed to the optimiser. In general, an optimisation problem is defined by an objective function $f(\mathbf{x})$, which is sought for minimum values, while satisfying a number of problem dependent constraints $g(\mathbf{x})$:

$$\begin{array}{lll} \text{Minimise} & f_m(\mathbf{x}), & m = 1,2,...,M; \\ \text{Subject to} & g_j(\mathbf{x}) \geq 0, & j = 1,2,...,J; \\ & x_i^l \leq x_i \leq x_i^u, & i = 1,2,...,n. \end{array} \tag{1}$$

where $\mathbf{x}$ is the design vector containing n design parameters $x_1,...,x_n$. The superscripts l and u define the lower and upper limit of a particular design parameter x_i. The details on how these parameters are defined in this work is described in a later section.

Initial Database - Design of Experiments

In order to carry out an optimisation and to explore the design space in an efficient way, it is necessary to start from an initial database. In this study, the initial database is created with a Design of Experiment (DOE) approach where the DOE is generated automatically using a Latin Hypercube sampling technique (LHS), which distributes a desired amount of initial database points homogeneously within the design space in such a way that each point is the only one in a certain axis-aligned hyperplane [19, 20]. From a stochastic point of view, this method provides the best interpolation dataset for an unknown behaviour of an objective function within a defined design space.

In order to choose the number of database points for the initial DOE, the recommendation given by Baerts *et al.* [21] is followed: for a purely continuous design space of a surrogate based optimisation, the authors took five times the number of design variables ($5 \times n$) for an initial DOE. This also seemed to be a reasonable approach for this study, due to the defined low dimensional space.

Surrogate Based Optimisation

For complex engineering problems, either 2D or 3D, the aim is to get to the optimum solution as fast as possible, i.e. with a minimum number of simulations. Therefore, mathematical or statistical approximation models are used to speed up the optimisation. In the technical literature, these models are known as surrogate models, metamodels or response surface models (RSM). In this study, the optimisation is conducted by using the so called Kriging technique, which is able to replicate accurately a complex multi-dimensional function. It is out of the scope of this paper to derive the equations in detail of the Kriging method. Therefore the reader is referred to the early literature of Krige [22] and Matheron [23] and for practical guidance in engineering to the book of Forrester *et al.* [24].

In this work regressing Kriging [25, 26] is used, which is based on the classical Kriging approach with an additional parameter to filter out scatter or noise coming from numerical calculations such as CFD. A schematic representation of the optimisation process based on Kriging as it is implemented in SOFT, can be seen in Fig. 2. Starting from an initial LHS DOE set, the obtained initial designs are evaluated in parallel and saved in a database or in case of failure, in a failure database. Once the designs are evaluated, a RSM is built using Kriging and the convergence of the RSM is checked using the efficient leave-one-out cross-validation method (see [26, 27]). If that is the case, the optimisation stops. Otherwise, the initial DOE is updated by additional points in order to iteratively get to a more accurate solution.

In order to refine the DOE and to find a new set of update points, the RSM is searched using global and local optimisation techniques. Therefore, two optimisation algorithms are chosen from the SOFT library: an adaptive range multi-objective genetic algorithm (ARMOGA) [28] and sequential quadratic programming (SQP) [29, 30]. The searching criteria follow a list of preferences until the maximum number of update points, also known as infill points, is reached (six points per update). First it is searched for the best constrained generalised expected improvement (CGEI) [24]. In a second step - if no CGEI could be found or the maximum number of update points is not yet reached - the maximum Kriging error is sought to find the location of maximum uncertainty. In a third step a search is made for the best Kriging prediction.

NUMERICAL METHODOLOGY

This section introduces the reader to the numerical methods used in this study. An introduction to the analysed test case geometry and its discretisation is given, followed by the parametric geometry definition and the definition of the optimisation parameters. The main assumptions and simplifications, which were necessary to set up the automated optimisation are also presented.

CFD Evaluation

The geometry used in this work is based on the MAGPI rig test facility, which has already been analysed thoroughly in recent years [3–6, 31–34]. For a full overview of the rig geometry with its instrumentation and running conditions the reader is referred to the work of Eastwood [34]. From a numerical point of view the experimental data was used to develop and validate reliable methods to predict both the flow phenomena in TSWs for different amounts of cooling mass flow, and also the conjugate heat transfer on the life critical rotor parts.

In order to keep the computational requirements within the capability of available computer facilities, it was decided to reduce the size of the discretised domain to a minimum. As in the previous numerical study on the original deflector plate geometry [6], in this work a 1/39th sector model was chosen, which is a reasonable approximation due to the periodicity of the 78 blades and 39 vanes per stage. Furthermore, the two stage domain was reduced to only one rotor blade pair from the first stage and the upstream cavity including the deflector plate until the first fin of the interstage seal. The rotational Reynolds number Re_ϕ is roughly 1.6×10^6.

The mesh was generated using the automatic Rolls-Royce in-house meshing tool PADRAM (see Fig. 3). The main annulus domain was generated using a multi-block structured approach, following the mesh sensitivity study of Dixon *et al.* [3], whereas the cavity was meshed in an hybrid unstructured way, following some assumptions made and verified for its suitability by Pohl *et al.* [6]. In order to generate the mesh automatically with PADRAM and to make it feasible for HYDRA the cavity domain was meshed in a single reference frame, meaning that the connecting bolt between stator

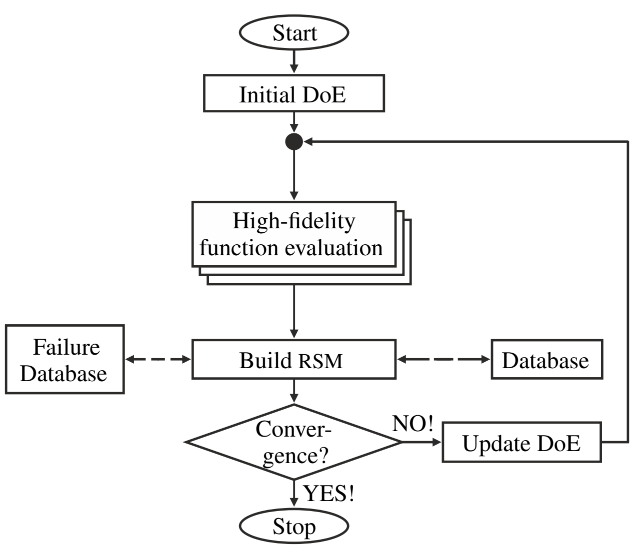

Figure 2. Schematic representation of the Optimisation strategy using Kriging in SOFT

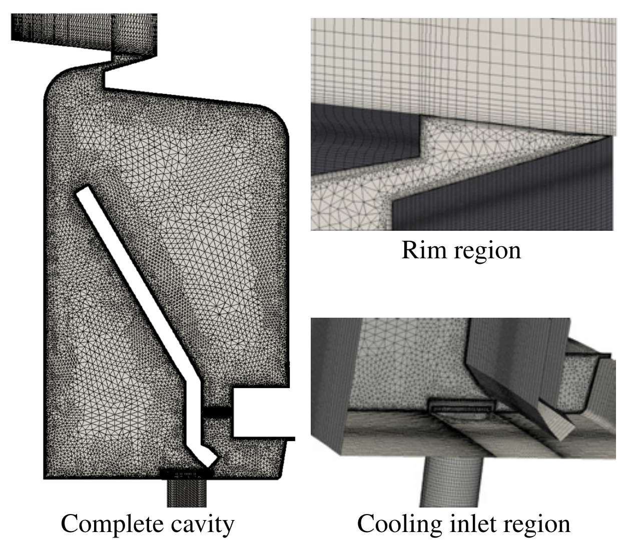

Figure 3. Mesh of upstream TSW cavity with deflector plate merged to the main annulus

foot and deflector plate was removed. Previous analyses have demonstrated that the bolt only affects the flow field locally and that perturbations in temperature and swirl can be considered minor.

The cavity mesh was then merged conformally at the rim to the main rotor mesh, which results in an overall mesh size of around six million cells. The boundary layer was resolved, ensuring y^+ values of around 1 in the most of the near wall regions. Only the regions around the first fin as well as at the stator and deflector plate, where the bolt used to connect both parts, did not match this criterion.

At this stage the Rolls-Royce in-house CFD code HYDRA was used to solve the RANS equations using a second order finite volume discretisation of the domain in double precision. The turbulence closure was done using the $k-\omega$ turbulence model with adaptive wall functions of Launder and Spalding [35] in the regions where the near wall resolution was large. The cooling air inlet was defined as a mass flow inlet with a fixed temperature. The inlet for the main annulus was defined as a pressure inlet, where the total pressure was read across from the solution of the complete main annulus. The same approximations were taken for the outlets in the main annulus and the fin, where the static pressure distributions were taken from the full sector model run. The walls were defined as adiabatic, to keep the computation within a reasonable time scale. During the early design phase of the MAGPI test rig, similar stand-alone adiabatic CFD simulations were carried out to get an idea of the impact on the disc temperature using different geometries and varying amounts of cooling air [3].

In order to validate the outcome of the optimisation using stand-alone adiabatic CFD, a well established coupled FEA/CFD method [36] was applied to the final geometry to extract metal temperatures. These results were based on the coupling between the in-house FEA solver SC03 and the commercially available CFD code FLUENT. The two codes communicate through a Rolls-Royce proprietary communication library. For details on the method and the FEA model with the deflector included it is referred to the work of Pohl *et al.* [6]. Both stand-alone CFD solutions from the two different CFD solvers, HYDRA and FLUENT, were compared beforehand. Since no significant differences were found in the temperature predictions inside the cavity, the change in between solvers was possible.

Parametric Geometry Definition

The cavity geometry and the rotor geometry were not changed in this study. Only the shape and the position of the deflector plate were modified. The parameterisation of the deflector plate was done in 2D and is shown in Fig. 4 (a). It was chosen to define the midsection of the deflector plate by four control points, defining three separate B-spline curves (1-3), which in this work were defined as straight lines. There were mainly two reasons for this: first, to make the parameterisation as general as possible by avoiding hard-coded values. Second, to generate a manufacturable solution, which also could be mounted to the stator foot, meaning that it was necessary to have a vertical curve 2.

The points of the B-splines of the midsection were then projected orthogonally in positive and negative direction with a distance of half the thickness $t/2$ of the deflector plate. It can also be seen that the angle of curves 1 and 2 did not have to be the same. The degrees of freedom of the four control points are depicted in Fig. 4 (b). In total seven geometrical design parameters were defined:

- $d_{U,x}$ and $d_{U,r}$, which define the axial and radial degree of freedom of the upper point
- $d_{D,x}$, which defines the axial distance of curve 2 to the stator foot
- $d_{D,r}$, which defines the radial degree of freedom of the point connecting curve 1 to curve 2 with respect to the outer radii of the stator foot
- l_D, which defines the length of curve 2
- $d_{L,x}$ and $d_{L,r}$, which define the axial and radial degree of freedom of the lower point

Before setting up the optimisation it was checked that the generated geometry after applying the thickness to the midsection would not cut or touch lines of the remaining non-changed cavity geometry. Second, checks were made to ensure that the most extreme geometries, i.e. the one with the tightest gaps between parts, could be reliably meshed in PADRAM without corrupting the defined boundary layer.

Optimisation Setup

In order to finally setup the automated optimisation loop, an objective function as well as the constraints have to be defined, both depicted in Fig. 4 (b) in blue and red, respectively. The objective of this optimisation is to minimise the cooling air

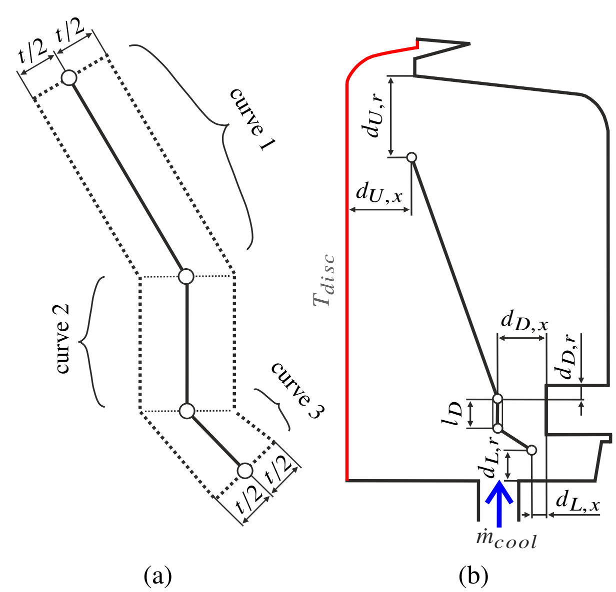

Figure 4. Definition of the geometrical parameters of the deflector plate: (a) shape definition, (b) position inside the cavity

mass flow rate entering the cavity through the drive arm hole and defined as follows:

$$f(\mathbf{x}) = \dot{m}_{cool} \tag{2}$$

with $\mathbf{x}$ being the design vector consisting of eight design parameters (seven geometrical and one for the cooling air mass flow rate). Also one constraint $g_j(\mathbf{x})$ is defined (see Fig. 4 (b)):

$$g_j(\mathbf{x}) = T_{disc}^{max} - T_{disc,j} \geq 0 \tag{3}$$

where T_{disc}^{max} is the maximum allowable area mean adiabatic wall temperature at the disc and $T_{disc,j}$ the computed value for a particular design j. The maximum value was taken from the results of a numerical simulation of the baseline geometry and an initial cooling mass flow rate of 55gs^{-1}.

The actual optimisation is conducted in parallel, where each CFD simulation is run on 24 cores. At first a DOE of 40 design points is generated ($n = 8$).

RESULTS AND DISCUSSION

Optimisation Results

This section gives an overview of the results of the optimisation. Fig. 5 shows the convergence history of the Kriging assisted optimisation, where the circles represent feasible and the crosses non-feasible solutions. A design is considered feasible when the solution stays within the limits of the constraint. Overall, 98 design points have been evaluated, where five mesh failures were recorded, one in the DOE and four in the optimisation process. Although, at first, only non-feasible designs were found, the optimiser managed to find feasible designs for small amounts of cooling air. The optimised deflector design only needs 19gs^{-1} of cooling air compared to 55gs^{-1} for the baseline geometry without deflector, which is a reduction of around 65%. Compared to the non-optimised deflector, where earlier studies showed that 30gs^{-1} achieves a similar performance to the baseline geometry [6], the optimised deflector reduces the coolant by another 40%.

A different representation of the evaluated results is presented in Fig. 6, where the amount of cooling air is plotted against the area mean averaged adiabatic wall temperature

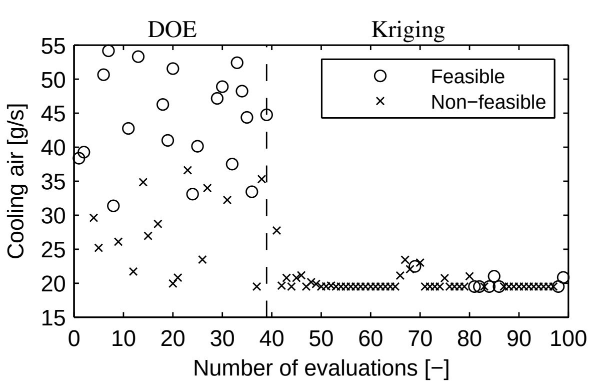

Figure 5. Convergence history of the Optimisation

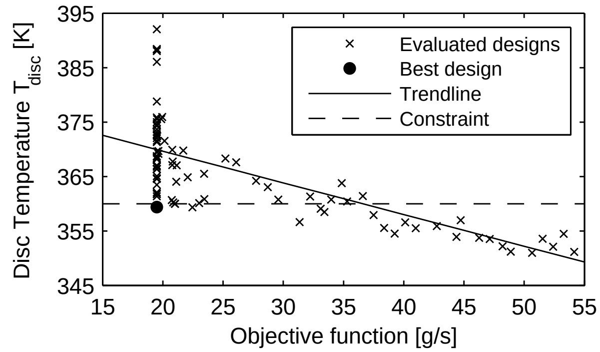

Figure 6. Objective function plotted against constraint for evaluated simulations

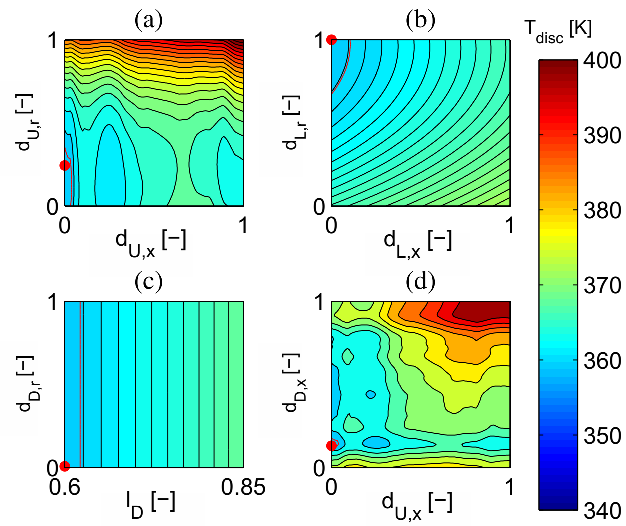

Figure 7. Overview of the Kriging prediction contoured by the temperature near the rotor disc T_{disc}

at the disc. The optimum design is highlighted by the black filled circle whereas the dashed line represents the constraint. All points below that line are considered feasible, the others non-feasible. A linear trend is observed in this representation. The cooling performance shrinks with a reduction of coolant air, as one would expect. Interestingly, for all cooling mass flow rates above the value of around 37gs^{-1} (cutting point between trendline and constraint), all deflector designs meet the required cooling performance of the disc.

Figures 7 (a) – (d) show the Kriging predictions coming from the optimisation for all geometrical design parameters. The response surfaces are obtained from the optimisation process as presented above. The four different plots are coloured by the near disc temperature T_{disc} and represent slices through the eight dimensional design space. With these plots it is possible to analyse the influence of each design parameter on the cooling performance of the disc. Examining the values of the optimised design, which are highlighted by the red dots, it is clearly visible that the optimiser moves the design points to the extreme values of the design space. Two design variables ($d_{U,r}$ and $d_{D,x}$ in Fig. 7 (a) and (d)) were optimised without reaching the limits of the design space. These variable define

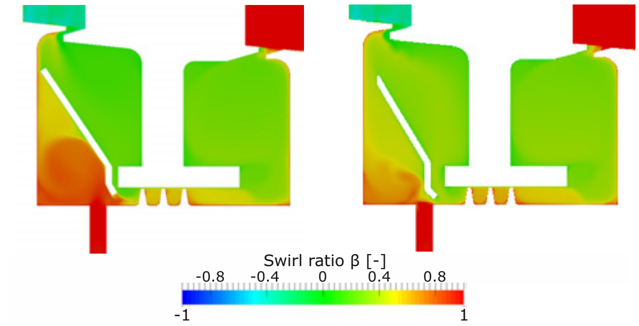

Figure 8. Contours of swirl ratio for the optimised (left) and non-optimised deflector plate (right) in a mid-plane cut

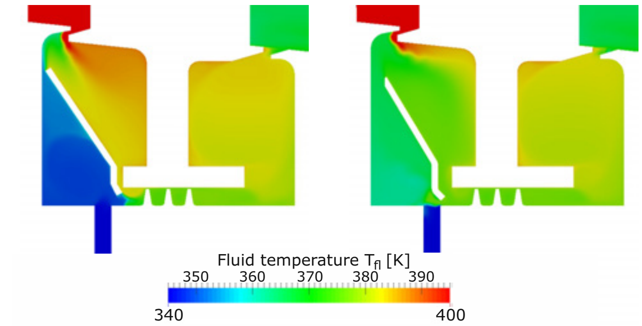

Figure 9. Contours of fluid temperature for the optimised (left) and non-optimised deflector plate (right) in a mid-plane cut

the radial position of the upper point and the axial position of curve 2 with respect to the stator foot. The upper point (Fig. 7 (a)) is moved axially as close as possible to the rotor disc whereas the lower point is moved radially as well axially to close proximity to the stator foot (Fig. 7 (b)). The length of the vertical curve 2 and the relative radial position with respect to the stator foot (Fig. 7 (c)) are also pushed to the lower design limits ($l_D = 0.6$ and $d_{D,r} = 0$).

From this information, the new position and design of the deflector was modelled and included in the complete two stage sector geometry. Steady-state adiabatic CFD were then carried out in order to analyse the optimised TSW flow in detail and to verify the outcome of the optimisation.

The Optimised Deflector Plate - Steady-State CFD

A comparison of the optimised deflector (left) against the non-optimised deflector (right) with respect to the position and shape based on the findings presented in the previous subsection can be seen in Figs. 8 and 9: the upper tip of the deflector is moved close to the rotor disc, whereas the lower parts are moved close to the stator foot. The depicted mid-plane cuts are contoured by swirl fraction β (= $\mathrm{v}_\theta(\omega\mathrm{r})^{-1}$) and relative total temperature. Both simulations were run with the reduced cooling mass flow rate of 19 g s^{-1}. For the optimised geometry, it can be seen that the cooling air enters the cavity swirled at disc speed ($\beta = 1$) and keeps its swirl as long as it does not impinge the deflector. This maintenance of swirl due to the position of the deflector close to the stator foot is beneficial for the cooling performance of the disc. Having a look at the non-optimised deflector, the cooling air loses all its swirl quickly after entering the cavity even before impinging the deflector. Another interesting phenomenon can be seen at the lower tip of the deflector plate, where - for the optimised design - part of the highly swirled cooling air seems to move to the interstage seal straight away without cooling the disc. This ensures that the gap between the deflector lower tip and the rotor wall is sealed against hot gas coming from higher radii. This is not the case for the non-optimised geometry.

Examining the temperature contours inside the cavity for the optimised design, it can be seen that the cooling air enters the cavity and then partially splits up, as one could infer from the swirl ratio contours. The disc is cooled all along the area enclosed by the deflector. It can also clearly be seen that hot gas from the main annulus ingests through the rim into the upstream cavity since the amount of cooling air does not meet the sealing requirements anymore. This results in a strong heat-up of the area between the deflector and the stator foot as well as the downstream cavity. The cooling air however does seal the region between the lower tip of the deflector and the rotor wall avoiding hot gas to enter the critical area between deflector and rotor disc.

In the non-optimised geometry, the air, which is used to cool the disc, is of higher relative total temperature than that in the optimised design. This is mainly due to two reasons: firstly, the cooling air loses all its swirl after entering the cavity, which results in an increase in relative total temperature. Secondly, the gap between the lower deflector tip and the rotor disc is not sealed, which results in hot air coming from higher radii entering the area between the deflector and the rotor disc. However, the air temperatures along the stator wall are slightly lower for the non-optimised design than those for the optimised one. While in the former the entire cooling flow penetrates the upstream cavity and mixes with the ingested flow, in the latter a fraction of the coolant is directly diverted towards the interstage seal.

Having analysed the steady-state CFD results for the optimised deflector, it can be concluded that the optimisation converged to a better deflector design, keeping the rotor disc cool while reducing the amount of cooling air. However, the fact that a large amount of hot gas enters the cavity, which inevitably results in a heat-up of the metal, needed further investigation. Therefore, coupled FEA/CFD analyses were carried out in order to extract the metal temperatures for the optimised design, the non-optimised deflector plate (both for a cooling air mass flow rate of 19 g s^{-1}) and the baseline design without a deflector (55 g s^{-1}). Also it is worth mentioning that the simulations were run with a constant interstage seal clearance only. The thermo-mechanical impact of the stator heating on the interstage seal clearance was not considered.

FEA/CFD Coupling - Metal Temperature Predictions

Figures 10 and 11 summarise the results of the FEA/CFD coupled analyses. In Fig. 10 contours of metal temperature of the optimised (left) and non-optimised deflector (middle) with a reduced cooling air mass flow rate of 19 g s^{-1} as well as the baseline geometry (right) with a cooling air mass flow rate of 55 g s^{-1} are depicted. Figure 11 shows a comparison of discrete metal temperature values from these models at the

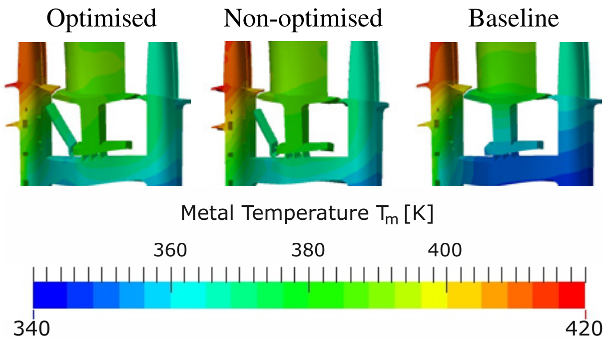

Figure 10. Metal temperature contours for three different geometries

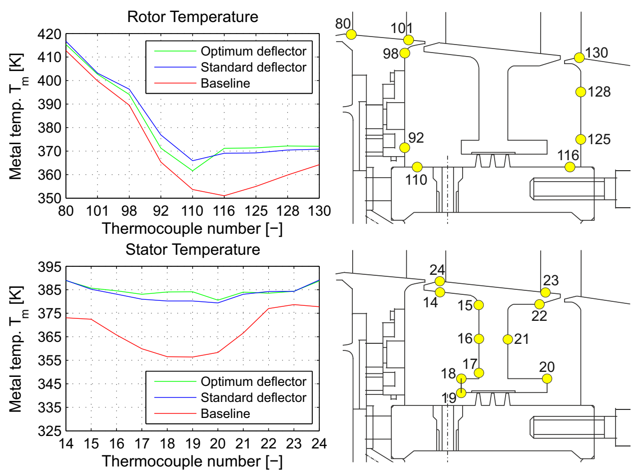

Figure 11. Comparison of metal temperatures

original thermocouple measurement points from the MAGPI rig [34]. From the contours and the plots, it can be seen that the temperatures inside the upstream rotor disc are very similar (positions 80, 101, 98, 92) for the optimised deflector and the baseline geometry, which was the requirement to the optimisation. The non-optimised deflector is slightly worse, especially at the lower radii of the rotor disc.

Then, moving further downstream inside the cavity (positions 110, 116, 125, 128, 130) the rotors of the deflector designs are hotter compared to the baseline geometry. A reason for that, as mentioned before, is due to the hot gas from the main annulus ingesting into the upstream cavity, which then heats up the interstage seal as well as the downstream cavity compared to the baseline geometry. This has also an effect on the metal temperature. Having a look at the temperature distribution along the rotor, it can be seen that despite the increase in temperature of the downstream rotor in the optimised design, the temperatures are still lower than in the upstream region. Hence, as a whole, from the thermal perspective, the optimised design with a reduced amount of cooling air is no worse than the baseline with the higher amount of cooling air. And for the same amount of coolant, the optimised deflector geometry performs better than the non-optimised deflector design.

The comparison of the stator metal temperatures shows larger differences between the deflector and the baseline designs due to the reasons mentioned above. Due to the hot gas ingestion, the stator temperatures are nearly constant over the radius and the axial position whereas in the baseline geometry the stator is cooled. Due to the higher amount of ingestion for the optimised design compared to the non-optimised deflector, the upstream stator (positions 16, 17, 18, 19) is also slightly hotter for the optimised deflector design, which also agrees with the findings from the steady-state CFD in the previous section. Since the stator foot is not a life limiting part and the temperatures are still lower compared to the rotating components, it can be concluded that the insertion of the optimised deflector provides an efficient distribution of cooling air inside the cavity, keeping the critical parts cool and the non-critical parts in a reasonable temperature range.

The comparison of the optimised to the non-optimised deflector design for this rig test case shows a small improvement in disc cooling and differences in the flow physics, which might be more significant for real engine running conditions, where temperatures as well as temperature gradients are much higher. Especially, the fact that ingested hot gas is able to pass through the gap between the lower deflector tip and the rotor disc for the non-optimised design, might cause life threatening conditions.

CONCLUSION

In this study an automated design optimisation using Kriging of a 3D sector model of a TSW test rig geometry with an inserted stationary deflector plate has been conducted. The geometry has been parameterised in such a way that flexibility of the design is ensured: different shapes and positions of the deflector plate inside the cavity have been generated automatically.

The outcome of the optimisation using adiabatic steady-state CFD has shown that the overall amount of cooling air can be reduced by approximately 65% compared to the baseline geometry without a deflector plate by still ensuring similar rotor disc cooling. This outcome has been verified using the coupled FEA/CFD method to compare metal temperatures for the new design to those for the baseline design. These results were in agreement with the stand-alone CFD results.

Another very important aspect for the new design and the reduced amount of cooling air is the fact that hot gas from the main annulus is ingested into the cavity, since the introduced amount of cooling air does not meet the sealing requirements of the cavity. This results in a metal temperature rise of the stator foot and also of the rotating downstream cavity components, but still keeps them at a temperature lower than the upstream components.

For future work in this research area, some recommendations are given here. When applying this method to real engine running conditions, it is essential - due to much higher temperatures and temperature gradients - to define an additional constraint to control and monitor the amount of ingested flow to the downstream cavity. Also the thermo-mechanical movements are of high importance. Not only, is it likely that a variation in seal size affects the final flow solution, but also the very extreme positions of the deflector should be chosen very carefully in order to prevent rubbing and damage at the most critical running conditions. The authors are also aware of the limitations of steady-state CFD in order to accurately predict the correct level of hot gas ingestion. For future work - in order to minimise these uncertainties - it is recommended to implement unsteady CFD or higher order turbulence models in the proposed optimisation strategy.

ACKNOWLEDGEMENTS

The present investigations were supported by the European Commission within the AMEDEO Marie Curie initial training network (grant reference 316394) and the authors want also to thank the European Commission for its support within the Framework 6 Programme, Research Project MAGPI, AST5-CT-2006-030874 for the use of the test rig geometry.

REFERENCES

[1] J. Illingworth, N. Hills, and C. J. Barnes. 3D Fluid-Solid Heat Transfer Coupling of an Aero-Engine Preswirl System. In *ASME Turbo Expo 2005, GT2005-68939*, Reno, Nevada, USA, June 2005.

[2] D. Amirante and N. Hills. A Coupled Approach for Aerothermal Mechanical Modelling for Turbomachinery. In *1st Int. Conf. on Computational Methods for Thermal Problems*, Napoli, Italy, September 2009.

[3] J. A. Dixon, A. Guijarro-Valencia, A. Bauknecht, D. Coren, and N. Atkins. Heat Transfer in Turbine Hub Cavities Adjacent to the Main Gas Path. *J Turbomach*, 135:021025–1–14, March 2013.

[4] R. DaSoghe, A. Andreini, and B. Facchini. Turbine Stator Well CFD Studies: Effects of Coolant Supply Geometry on Cavity Sealing Performance. *J Turbomach*, 133:021008–1–11, April 2011.

[5] D. D. Coren, N. R. Atkins, C. A. Long, D. Eastwood, P. R. N. Childs, A. Guijarro-Valencia, and J. A. Dixon. The Influence of Turbine Stator Well Coolant Flow Rate and Passage Configuration on Cooling Effectiveness. In *ASME Turbo Expo 2011, GT2011-46448*, Vancouver, Canada, June 2011.

[6] J. Pohl, V. Fico, and J. A. Dixon. Turbine Stator Well Cooling - Improved Geometry Benefits. In *ASME Turbo Expo 2015, GT2015-42658*, Montréal, Canada, June 2015.

[7] C. Young, G. D. Snowsill, P. W. Ferra, and C. P. Gravett. Turbine apparatus. Patent number: US8186938, May 2012. PatBase number: 41140158.

[8] S. Shahpar, A. Polynkin, and V. Toropov. Large Scale Optimization of Transonic Axial Compressor Rotor Blades. In *AIAA Paper 2008-2056*, Schaumburg, Illinois, USA, April 2008.

[9] A. Polynkin, V. Toropov, and S. Shahpar. Multidisciplinary Optimization of Turbomachinery Based on Meta-Model Built bt Genetic Programming. In *AIAA Paper 2010-9397*, Fort Worth, Texas, USA, September 2010.

[10] R. C. Schlaps, S. Shahpar, and V. Gümmer. Automatic Three-Dimensional Optimisation of a Modern Tandem Compressor Vane. In *ASME Turbo Expo 2014, GT2014-26762*, Düsseldorf, Germany, June 2014.

[11] T. Verstraete, F. Coletti, J. Bulle, T. Vanderwielen, and T. Arts. Optimization of a U-Bend for Minimal Pressure Loss in Internal Cooling Channels - Part I: Numerical Method. *J Turbomach*, 135:051015–1–10, September 2013.

[12] H. Lück, M. Schäfer, and H.-P. Schiffer. Thermal Fluid-Structure Interaction Based Optimization of Secondary Air Flows in Rotor Stator Cavities of Aircraft Turbines. In *WCCM-ECCM-ECFD 2014*, Barcelona, Spain, July 2014.

[13] U. P. Phadke and J. M. Owen. Aerodynamic Aspects of the Sealing of Gas Turbine Rotor-Stator Systems - Part 1: The Behaviour of Simple Shrouded Rotating Disk Systems in Quiescent Environment. *Int J Heat Fluid Flow*, 9:98–105, 1988.

[14] U. P. Phadke and J. M. Owen. Aerodynamic Aspects of the Sealing of Gas Turbine Rotor-Stator Systems - Part 2: The Behaviour of Simple Seals in Quasi-Axisymmetric External Flow. *Int J Heat Fluid Flow*, 9:106–112, 1988.

[15] S. Shahpar. SOPHY: An Integrated CFD Based Automatic Design Optimisation System. Report No. ISABE-2005-1086, 2005.

[16] S. Shahpar. SOFT: A New Design And Optimisation Tool for Turbomachinery. In K. Ginnakoglou et al., editor, *CIMNE 2002*, Athens, Greece, 2002.

[17] S. Shahpar and L. Lapworth. PADRAM: Parametric Design and Rapid Meshing System for Turbomachinery Optimisation. In *ASME Turbo Expo 2003, GT2003-38698*, Atlanta, Georgia, USA, June 2003.

[18] L. Lapworth. Hydra-CFD: A Framework for Collaborative CFD Development. In *IC-SEC*, Singapore, July 2004.

[19] M. D. McKay, W. J. Conover, and R. J. Beckman. A Comparison of Three Methods for Selecting Values of Input Variables in the Analysis of Output from a Computer Code. *Technometrics*, 21(2):239–245, 1979.

[20] M. Stein. Large Sample Properties of Simulations Using Latin Hypercube Sampling. *Technometrics*, 29(2):143–151, 1987.

[21] L. Baert, C. Beauthier, M. Leborgne, and I. Lepot. Surrogate-Based Optimisation for a Mixed-Variable Design Space: Proof of Concept and Opportunities for Turbomachinery Applications. In *ASME Turbo Expo 2015, GT2015-43254*, Montréal, Canada, June 2015.

[22] D. G. Krige. A Statistical Approach to Some Basic Mine Valuations and Allied Problems at the Witwatersrand. Master's thesis, University of Witwatersrand, South Africa, 1951.

[23] G. Matheron. Principles of Geostatistics. *Economic Geology*, 58:1246–1266, 1963.

[24] A. I. J. Forrester, A. Sobester, and A. J. Keane. *Engineering Design via Surrogate Modelling: A Practical Guide*. Wiley, Chichester, 2008.

[25] A. I. J. Forrester, A. J. Keane, and N. W. Bressloff. Design and Analysis of "Noisy" Computer Experiments. *AIAA Journal*, 44(10):2331–2339, 2006.

[26] C. J. Brooks, A. I. J. Forrester, A. J. Keane, and S. Shahpar. Multi-Fidelity Design Optimisation of a Transonic Compressor Rotor. In *9th European Conference for Turbomachinery, Fluid Dynamics and Thermodynamics*, Istanbul, Turkey, March 2011.

[27] O. Dubrule. Cross Validation of Kriging in Unique Neighbourhood. *Math. Geol.*, 15(6):687–699, 1983.

[28] D. Sasaki and S. Obayashi. Efficient Search for Trade-Offs by Adaptive Range Multi-Objective Genetic Algorithms. *J. Aeros. Comp. Inf. Com.*, 2:44–64, 2005.

[29] P. E. Gill, W. Murray, and M. H. Wright. *Practical Optimization*. Academic Press, 1981.

[30] M. J. D. Powell. Variable Metric Methods for Constrained Optimization. In A. Bachem, B. Korte, and M. Grätschel, editors, *Mathematical Programming: The State of the Art*, pages 288–311. Springer, Berlin, Heidelberg, 1983.

[31] A. Guijarro-Valencia, J. A. Dixon, R. Da Soghe, B. Facchini, P. E. J. Smith, J. Munoz, D. Eastwood, C. A. Long, D. Coren, and N. R. Atkins. An Investigation Into Numerical Analysis Alternatives For Prediciting Re-Ingestion in Turbine Disc Rim Cavities. In *ASME Turbo Expo 2012, GT2012-68592*, Copenhagen, Denmark, June 2012.

[32] D. Eastwood, D. D. Coren, C. A. Long, N. R. Atkins, P. R. N. Childs, T. J. Scanlon, and A. Guijarro-Valencia. Experimental Investigation of Turbine Stator Well Rim Seal, re-Ingestion and Interstage Seal Flows Using Gas Concentration Techniques and Displacement Measurements. *J Turbomach*, 134:082501–1–9, August 2012.

[33] J. A. Dixon, A. Guijarro-Valencia, D. Coren, D., and C. Long. Main Annulus Gas Path Interactions - Turbine Stator Well Heat Transfer. *J Turbomach*, 136:021010–1–16, February 2014.

[34] D. Eastwood. *Investigaton of Rim Seal Exchange and Coolant Re-Ingestion in Rotor Stator Cavities Using Concentration Techniques*. PhD thesis, University of Sussex, Sussex, UK, 2014.

[35] B. E. Launder and D. B. Spalding. The Numerical Computation of Flows. *J Comp Meth Appl Mech Eng*, 3:269–289, 1974.

[36] J. A. Verdicchio. *The Validation and Coupling of Computational Fluid Dynamics and Finite Element Codes for Solving Industrial Problems*. PhD Thesis, University of Sussex, Sussex, UK, July 2001.